CASL-U-2015-0189-000

# Evaluation of Missing Pellet Surface Geometry on Cladding Stress Distribution and Magnitude

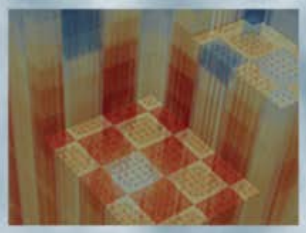

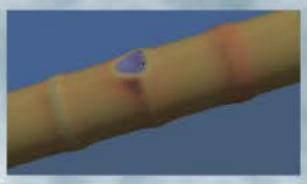

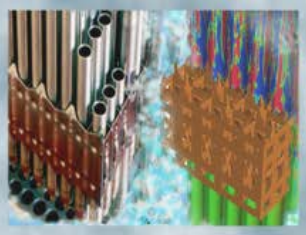


Nathan Capps and Brian D. Wirth
*University of Tennessee*

Robert Montgomery and Dion Sunderland
*Pacific Northwest National Laboratory*

Benjamin Spencer
*Idaho National Laboratory*

Martin Pytel
*Electric Power Research Institute*


**May 1, 2015**

www.casl.gov

## REVISION LOG

| Revision | Date | Affected Pages | Revision Description |
|---|---|---|---|
| 0 | | All | Initial Release |
| | | | |
| | | | |
| | | | |

**Document pages that are:**

Export Controlled _____

IP/Proprietary/NDA Controlled_____

Sensitive Controlled_____

**Requested Distribution:**

To:

Copy:

## Table of Contents

# Table of Figures

# EVALUATION OF MISSING PELLET SURFACE GEOMETRY ON CLADDING STRESS DISTRIBUTION AND MAGNITUDE

Nathan Capps[*1], Robert Montgomery[2], Dion Sunderland[2,3], Benjamin Spencer[4], Martin Pytel[5], and Brian D. Wirth[1]

[1] *Department of Nuclear Engineering, University of Tennessee, Knoxville, TN 37996*

[2]*Pacific Northwest National Laboratory, Richland, WA 99354*

[3] *ANATECH Corp, San Diego, CA 92121*

[4]*Idaho National Laboratory, Idaho Falls, ID 83401*

[5]*Electric Power Research Institute, Palo Alto, CA 94304*

***ABSTRACT:*** Missing pellet surface (MPS) defects are local geometric defects in nuclear fuel pellets that result from pellet mishandling or manufacturing. The presence of MPS defects can cause clad stress concentrations that are substantial enough to produce through-wall cladding failure for certain combinations of fuel burnup, and reactor power level or power change. Consequently, the impact of potential MPS defects has limited the rate of power increase, or ramp rate, in both pressurized and boiling water reactors (PWRs and BWRs, respectively). Improved three-dimensional (3-D) fuel performance models of MPS defect geometry can provide better understanding of the probability for pellet clad mechanical interaction (PCMI), and correspondingly the available margin against cladding failure by stress corrosion cracking (SCC). The Bison-CASL fuel performance code has been developed within the Consortium of Advanced Simulations of Light Water Reactors (CASL) to consider the inherently multi-physics and multi-dimensional mechanisms that control fuel behavior, including cladding stress concentrations resulting from MPS defects. This paper evaluates the cladding hoop stress distributions as a function of MPS defect geometry and the presence of discrete pellet cracks for a set of typical operating conditions in a PWR fuel rod. The results are a first step in a probabilistic approach to assess cladding failure during power maneuvers. This analysis provides insight into how varying pellet defect geometries affect the distribution of the cladding stress, as well as the temperature distributions within the fuel and clad; and are used to develop stress concentration factors for comparing 2-D and 3-D models.

***KEYWORDS:*** *Pellet Cladding Interaction (PCI), 3D fuel modeling and simulation, Pellet Cladding Mechanical Interaction (PCMI), missing pellet surface defects, Stress Corrosion Cracking (SCC)*

# 1. INTRODUCTION

Pellet cladding interaction (PCI) in light water reactor (LWR) fuel is a coupled thermal-chemical-mechanical process that can lead to cladding breach and release of radioactive fission products into the coolant under certain conditions of operating history, power change, and fuel rod design characteristics [ref. from TOP FUEL 2014 paper]. Reactor operating restrictions, which limit power maneuvering, have been established to mitigate PCI, but they restrain operational flexibility and lead to loss of power generation. The Consortium for the Advanced Simulation of Light water reactors (CASL) has selected PCI as a key challenge problem and is developing an advanced, 3-dimensional fuel rod simulation capability (referred to as Bison-CASL) to evaluate fuel performance, and in particular, provide PCI failure assessments. With an advanced fuel rod modeling capability that considers the underlying mechanisms leading to cladding failure, fuel designers and engineers can investigate improved fuel concepts for PCI-resistance and better quantify margins to PCI for existing fuel operation.

PCI failures generally occur following an increase in the local power over a short period of time and in fuel that has been previously exposed to irradiation. Classical PCI is driven by the localized strains in the vicinity of a pellet crack, as well as the presence of a chemical species, such as iodine, that drive stress corrosion-induced cracking of the cladding [ref]. Fuel pellet cracks, which are induced in the brittle ceramic by strong temperature gradients, are also believed important in the PCI failure mechanism [ref]. During a local power increase, pellet expansion produces a high contact force between the fuel and clad. Furthermore, during the rapid thermal expansion of the pellet, the fuel cracks can further open, which transfers tangential shear forces onto the cladding. These tangential shear forces are a function of the equilibrium pellet-clad gap or residual contact pressure at the start of the power increase, the power level at gap closure, the interfacial friction, and the maximum local power.

Non-classical PCI failure is associated with the presence of a missing pellet surface (MPS) defect [ref]. These MPS defects form through mishandling or the manufacturing process, where the pellet is chipped leaving a residual flaw in the outer surface. The presence of an MPS defect during a localized power ramp can cause severe bending moments in the clad in the vicinity of the MPS when the fuel undergoes rapid thermal expansion due to a power increase. Furthermore, the localized region near the MPS also experiences a different temperature distribution with a localized hot spot in the fuel and cold spot in the clad.

Both classical and non-classical PCI are significantly influenced by the geometric flaw geometry (i.e pellet cracks and MPS) of the fuel pellet. The purpose of the current paper is to assess the capability of Bison-CASL to be used as a 3-D fuel performance code to represent the underlining mechanisms controlling the failure of the cladding as a result of PCI. The assessment includes several activities to evaluate the thermo-mechanical modeling capabilities in Bison-CASL to calculate the localized cladding stress and temperature distribution in the vicinity of pellet cracks or defects. These geometric irregularities are known to cause stress intensification during pellet-cladding mechanical interaction (PCMI) that arises during local power increases in irradiated fuel. The ability to accurately calculate the local cladding stress concentration and temperature distribution is a critical component within any PCI failure analysis methodology, and establishing the assumptions used to represent geometric irregularities, material properties, and the numerical complexities of modeling contact and friction was the primary focus of this paper.

The assessment consisted of four major areas of investigation: 2-D geometric modeling of fuel pellet cracks, 2-D geometric modeling of missing pellet surface (MPS) defects, 3-D geometric modeling of fuel pellet cracks, and 3-D geometric modeling of MPS defects. As will be explained below, the forces causing cladding stress concentrations are different in the case of a fuel pellet crack impinging on the cladding or in the presence of an MPS defect. Therefore it is important to evaluate the approach required to capture these

effects within the computation model. Factors that were studied included the length and frequency of pellet cracks, the friction coefficient between the pellet and cladding surfaces, the size, length, and shape of the MPS defect, the approach to account for out-of-plane mechanical loading conditions for the 2-D geometric models, and finally, the role that 3-D modeling will have on the local cladding stress distribution. Earlier research performed by EPRI, CEA, and others [3, 4, 5] to develop modeling approaches to calculate the effects of pellet cracks and MPS defects using 2-D and 3-D methods was used to guide and validate the Bison-CASL assessment. In particular, the Bison-CASL calculations of cladding stress distribution and stress intensity factors have been compared to the same or similar analyses performed using the EPRI Falcon code, as well as 3-D modeling efforts using general-purpose finite element calculations in ABAQUS and ANSYS. The later results were obtained from prior efforts carried out by EPRI and AREVA.

Conditioning of the nuclear fuel refers to the state of the fuel rod with respect to the evolutionary changes in the fuel, the cladding and the fuel-cladding gap as a function of burnup and local power, and the ability of the fuel system to respond to rapid changes in local power without failure due to PCI. A 'conditioned' fuel rod is one that can withstand rapid power changes without cladding failure due to PCI. Conditioning of the fuel (or pre-conditioning and de-conditioning) is a consequence of the fundamental changes in fuel pellets and cladding as a function of irradiation, which is both time and exposure dependent. These changes include pellet cracking and relocation, fuel densification and/or swelling, which is driven by both solid and gaseous fission products, as well as grain growth in the fuel and creep deformation of both the fuel and clad.

During the first rise to power, ceramic fuel pellets are subject to thermal gradients due to the poor thermal conductivity of $UO_2$, which result in differential thermal expansion and induces tensile stresses in the outer regions of the pellet. When the local stress exceeds the fracture stress, the fuel pellet cracks, and the crack propagates inward. While major cracks are radially oriented, some cracking is circumferentially or transversely oriented as shown in Figure 1 [15]. The cracking allows the fuel fragments to move outward consuming part of the fuel-cladding gap, and improves the compliance of the pellet when it makes contact with the cladding. As irradiation progresses, some initial porosity disappears, as the pellets initially densify and shrink from the cladding, however eventually, the accumulation of fission products cause the ceramic material to swell.

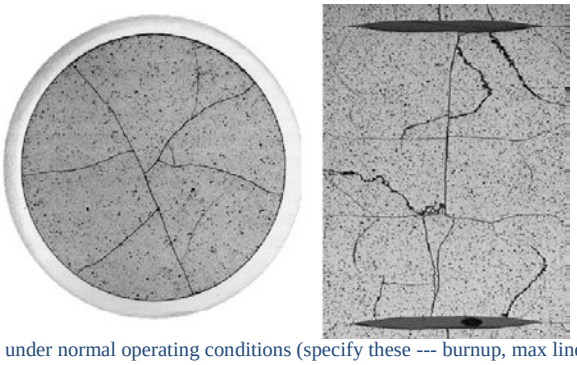

**Figure 1.** Fuel pellets irradiated under normal operating conditions (specify these --- burnup, max linear power, etc), as reproduced from Ref [15].

Simultaneously with the changes in the fuel, the cladding creeps (displaces) by irradiation-induced mechanisms inward under the influence of the external coolant pressure. Eventually, the cladding will make contact with the fuel pellet, and both will achieve a mechanical equilibrium at some power level.

Deconditioning refers to the relaxation of the cladding toward or onto the fuel at some reduced power level such that when a power increase occurs, the cladding experiences a significant tensile stress. At the same time, increased fuel temperatures allow for increased mobility of volatile fission products, such as iodine to travel along cracks from the pellet interior to the cladding surface. The nominal local stress in the cladding is intensified in the presence of fuel pellet cracks, when the cladding is in hard contact with the fuel, and a crack opens, or when there is a sufficiently large fuel or cladding flaw. In the presence of high tensile stress (above some critical threshold) and sufficient iodine activity, zirconium alloys experience stress corrosion cracking, PCI.

## 1.1 PCI Modeling Efforts

Traditional efforts to model fuel rod performance generally use a one, or one and a half dimensional (1/1.5-D) geometry representation of the fuel rod. This approach represents the fuel as a cylinder divided in slices and enclosed by a concentric cladding tube, which is also treated as slices, as shown in Figure 2 [16]. The 1-D codes use either analytical solutions or finite difference calculations to solve the heat conduction across the pellet, pellet-clad gap, and the cladding. Furthermore, burnup and fission gas release are calculated from these slices and an average value is reported. Typically, such codes are used to verify specified acceptable fuel design limits (SAFDLs) and provide fuel conditions for various licensing and safety analysis. Such codes assume uniform, axisymmetric geometric properties in the fuel, and thus are not suited to model the effects of asymmetries such as pellet flaws.

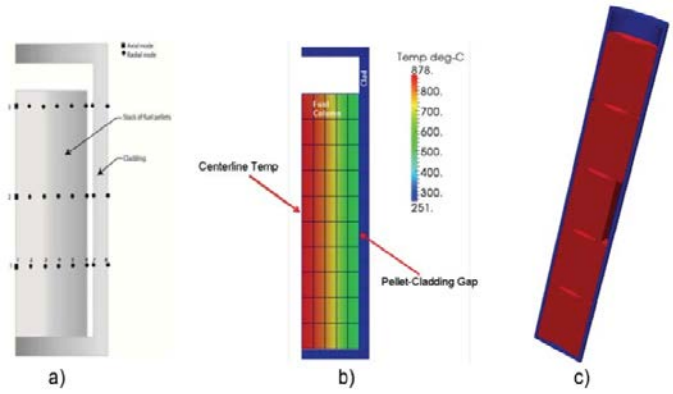


**Figure 2.** 1/1.5D-2D R-Z (a) 1/1.5-D Geometric Representation, (b) Falcon or Bison-CASL 2-D R-Z Fuel Rod Representation, and (c) 3-D Bison-CASL 5-Pellet Model Containing a MPS and the Cladding [16].

To improve the fidelity of the solution, finite element codes have been used to perform two-dimensional (2-D) axisymmetric R-Z, Figure 2 (b), and planar R-Theta geometric analysis, Figure 3 [16]. By

utilizing the finite element method, detailed information on the temperature, burnup and other material properties can be evaluated at integration or quadrature points on each element, and provide the ability to calculate local stress concentrations.

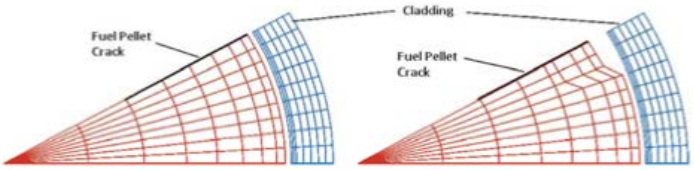


**Figure 3.** Falcon representation of a fuel pellet and cladding containing a crack and a MPS in the fuel in R-Theta space, as reproduced from Reference [16].

More than 30 years ago, it was recognized by Gittus and others that axi-symmetric 1-D and 2-D fuel codes with smeared fuel columns are unable to treat non-uniform geometric affects present in fuel pellets [9,17,18]. The local stress and strain concentrations associated with pellet cracks impinging on the cladding where shown to be 150 to 300% of the mean cladding stress using analytical approaches. These intensity factors were dependent on several critical parameters, including the pellet-cladding friction coefficient, the fuel crack opening displacement, and the cladding mechanical properties. Rashid and others began to develop approaches based on the finite element method to calculate the time dependent behavior of the local stress and strain concentrations to better represent the impact of material creep on the PCI failure [4, 5]. Fuel performance codes such, as Falcon and ALCYONE, have been developed to model a slice of a fuel pellet in a 2-D, R-Theta geometric representation, as shown in Figure 3 [4, 16]. Such a planar representation allows for treatment of discontinuities in the circumferential direction that can cause local perturbations in the fuel and cladding stress and temperature distributions.

The use of 2-D R-Theta geometric representation of the critical location on a fuel rod has been used successfully in root cause failure analysis of PCI-suspected fuel rods and to establish operating guidance for plants affected by MPS defects [2, 11]. However, this method still has a number of limitations that impact the ability of 2-D modeling to accurately model the conditions leading the cladding failure by PCI mechanisms. These include; 1) the need for a full-length R-Z fuel performance calculation to establish and provide the evolution of the fuel pellet and clad conditions as a function of prior operating history, 2) approximation of the out-of-plane mechanical and thermal boundary conditions (plane strain vs. plane stress), and 3) the fact that the geometric defects are infinitely long in the out-of-plane direction. To capture the inherent 3-D geometric affect of a defect in a pellet as well as other unique pellet deformations, such as hour glassing, finite element analysis (FEA) based structural codes (which are not multiphysics codes) such as ABAQUS [19] and ANSYS [20] have been used to determine correction factors that can be applied to 2-D results. Unfortunately, using a structural analysis approach may miss the impact of important phenomena such as fuel and cladding creep, fission gas swelling and release, and burnup on the evolution of the cladding stress.

FEA allows a user to simulate cracks discretely, or numerically as ‘smeared cracking’. In R-Z geometry, smeared cracking is employed for all cracks, whereas in R-theta and R-theta-Z, discrete cracks may be modeled explicitly, with the effects of transverse and circumferential cracks modeled with smeared

cracking. So far, relocation has been treated separately and independently, although it is the goal of the Bison-CASL development to couple relocation to the smeared cracking model.

These factors highlight the importance of developing a fully integrated 3-D fuel performance code and analysis methodology to accurately calculate the conditions leading to cladding failure by both classical and non-classical PCI mechanisms. By developing a 3D fuel performance modeling capability, key local effects can be studied and understood within a single analysis. In particular, within a 3-D analysis of a fuel rod, pellet defects including discrete cracks and MPS can be modeled simultaneously with capturing the irradiation history.

## 2. MODELING APPROACH

The objective of developing an advanced, 3-D fuel performance modeling capability to assess PCI is to: 1) reliably calculate the cladding failure potential related to PCI; 2) define the impact of manufacturing flaws along with the material properties on failure probability; and 3) to evaluate the role of plant operating strategies as well as specific fuel designs on the PCI failure potential. To meet these objectives, it is imperative to develop a high-fidelity, fully coupled computer code that incorporates important plant operating procedures, e.g. power ramp rate and axial power shapes related to fuel performance, as well as considering the inherently coupled intricacies that occur in irradiated fuel behavior during normal and transient operations. By developing and employing a advanced fully coupled multi-physics and multi-dimension fuel performance code and developing mechanistic or physics based material models, efforts can be taken to reduce the uncertainties surrounding existing PCI failure methods. The approach to address the current uncertainties in PCI failure probabilities will allow for improved fuel utilization and increase the plant operating flexibility.

Again, the focus of the current article is to assess the capability of Bison-CASL as a 3-D fuel performance code to represent the underlining mechanisms controlling the failure of the cladding as a result of PCI. As mentioned in Section 1, the processes leading to cladding crack initiation and propagation begins with the presence of localized stress and strains in concert with available corrosive fission products. PCI fuel behavior modeling must be built upon a methodology that can reliably and consistently calculate the local stress conditions as a function of prior irradiation history, material properties, and local power conditions. This means capturing the effects of geometric irregularities (i.e. pellet cracks), permanent changes in dimensions of the pellet and cladding caused by fission product swelling and irradiation-induced cladding creep, as well as, thermal, mechanical, and chemical interactions between the pellet and cladding, i.e. frictional forces, heat transfer, and chemical bonding.

The assessment first focuses on the approach to model pellet cracks and MPS defects using a 2-D planar geometric representation (R-theta model) in order to capture the impact of these geometric irregularities on the localized cladding stress and temperature distribution. Several, including EPRI [ref], have used a 2-D approach to calculate pellet-cladding mechanical interaction as part of a PCI analysis methodology. Therefore, starting with a 2-D approach allows for both quantitative and qualitative comparisons to previous results from others, providing assurance that the capabilities in Bison-CASL are consistent with established methodologies. The 2-D modeling in Bison-CASL was used to investigate the impact of pellet crack radial length as well as pellet crack frequency on cladding stress localization. In the case of a MPS defects, the 2-D approach was used to quantify the influence of the MPS defect shape (width and depth) on the cladding stress and fuel temperature distribution. Concentrating on modeling PCMI using a 2-D planar approach allows for a learning process to be conducted where the influence of assumptions, finite element mesh restraints, and other factors can be exercised without incurring the difficulties of 3-D modeling

approaches. These 2-D investigations will provide a foundation of understanding that can be used to support the ultimate goal of 3-D modeling in Bison-CASL.

In addition to the 2-D investigations, a set of 3-D simulations were performed to: 1) support the 2-D modeling by providing out-of-plane mechanical conditions, 2) evaluate candidate approaches for representing discrete pellet cracks and MPS defects in three dimensions, and 3) identify the areas of improvement needed in Bison-CASL or the MOOSE framework to reliably calculate localized PCMI as realistically as possible. The 3-D modeling activities were limited to a single pellet or short stack of pellets (3-5 pellets) to conserve computational resources and simplify the complexities of modeling full-length fuel rods in three dimensions.

## 2.1 Bison-CASL

Bison-CASL is built upon the Multi-physics Object-Oriented Simulation Environment (MOOSE) [21] developed at Idaho National Laboratory (INL). MOOSE is a massively parallel finite element computational system that uses a Jacobian-free, Newton-Krylov (JFNK) method to solve coupled systems of non-linear partial differential equations. In addition, the MOOSE framework provides the ability to effectively use massively parallel computational capabilities needed to create high fidelity 3-D models of a fuel rod, as well as full-length R-Z rods, and R-Theta geometric representation.

Bison-CASL builds upon the underlying architecture of BISON, developed at INL [3]. This architecture includes the ability to incorporate, or develop, material properties libraries and fuel behavior models for $UO_2$ fuel and zirconium alloy cladding commonly used in PWRs. A major focus of the CASL effort on modeling nuclear fuel performance, beyond the Bison-CASL development, has been to develop physics-based material models for ceramic $UO_2$ fuels and zirconium alloys [16]. These models consist of irradiation induced clad creep and growth, clad corrosion, the hydrogen pickup and hydride precipitation in the clad, and the release and transport of fission gas. However, since Bison-CASL is being developed simultaneously with the effort to develop improved mechanistic behavior models that are not yet ready for implementation, empirical models from the open literature and selected EPRI/Falcon models have been incorporated to date. This allows for testing of the numerical framework of Bison-CASL, as well as to identify material models that require further development.

## 2.2 Modeling Approach

A key goal in developing Bison-CASL is to be able to model a fully coupled, 3-D pellet containing radial cracks and/or MPS defect, calculate stresses in the cladding, and ultimately incorporate a mechanistic stress corrosion cracking (SCC) model to determine the potential for cladding fracture. Achieving this goal requires developing a foundation from a 2-D planar approach and working towards 3-D geometric representation. First, sensitivity studies have been conducted using 2-D R-Theta planar geometries of the pellet and cladding to understand the effect of the depth and frequency of discrete fuel pellet cracks on the localized cladding hoop stress. These studies evaluate different approaches to representing the stochastic nature of fuel cracks. The use of a 2-D geometric representation in the R-Theta plane circumvents the difficulties of solution convergence associated with 3-D contact of cracked bodies and allows for a large number of simulations under different conditions to improve understanding of the impact of geometric flaws on the localized stress and temperature distributions.

The R-Theta geometric models are based on an AP-1000 fuel rod design, for which a 70% reduction in the gap size was used to simulate the pellet swelling and cladding creep down at a local burnup of about 20 GWd/tU. Furthermore, an initial fast fluence of 5e25 n/m$^2$ is applied to the cladding to account for the material property changes at this exposure. To evaluate the impact of discrete radial pellet cracks on the local clad hoop stress, we have used a quarter-symmetry, or 90 degree, model containing 2, 3, or 4 radial cracks with a crack length of 50% of the pellet radius, as shown in Figure 4 (a). A similar method was used to assess the role of the crack length on the maximum cladding hoop stress. The cracks in Figure 4 (a) are considered to be free surfaces. By considering the cracks as free surfaces, it allows for them to open during an increase in thermal gradient and relax while at constant power. This provides the basis for the cracks to impose shear stresses on the cladding during a power maneuver. In order to evaluate the role of MPS defects on cladding failure during power operation, analysis of the MPS size and its impact on the clad hoop stress has been performed using a 180°, or one half symmetry, 2-D R-Theta model, which contains three discrete radial cracks and an MPS defect, as shown in Figure 4 (b).

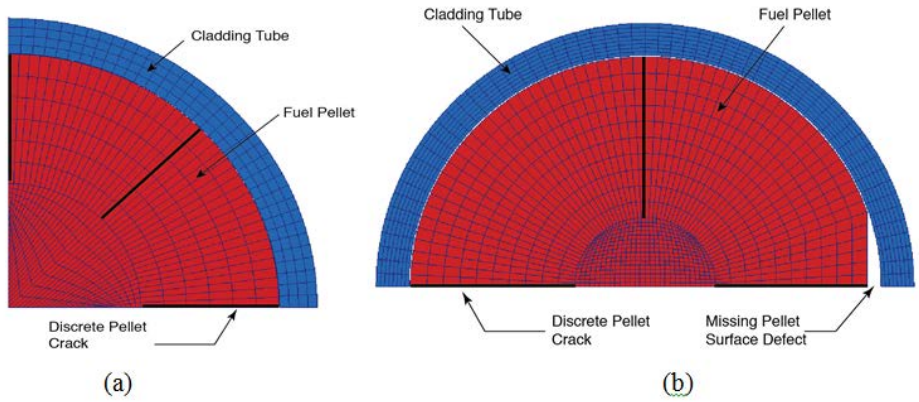


**Figure 4.** (a) 2-D, R-Theta model showing a representative three crack geometry (at 0, 45 and 90°, respectively) of radially oriented hald-length cracks in the fuel pellet, and (b) Geometric representation of an MPS defect in 2-D R-Theta space.

The 2-D simulations (in R-Theta) provide results needed to develop a methodology to mechanistically model the geometric effects of pellet cracks and MPS defects. However, the 2-D simulations are only able to capture the planar effects of localized pellet defects, and are unable to capture the inherently 3-D aspects of MPS defects or pellet cracks. Such axial effects involve axial power variations and hour glassing that cannot be captured in a 2-D R-Theta model. A similar methodology is used to evaluate classical PCI as well as the impact of an MPS defect on the clad hoop stress, with the exception that the MPS geometry is now a function of width and length, and the pellet cracks are assumed to run through the length of the pellet. Figure 5 (a) shows a 1/8$^{th}$ 3-D geometric model for a single pellet containing three radial cracks surrounded by a concentric cylindrical cladding tube, and Figure 5 (b) shows a one-half (180º) 3-D geometric model of a five-pellet rodlet in which the center pellet contains an MPS defect. Furthermore, there are 2 radial cracks in the five-pellet model, which run along the symmetry plane.

The treatment of contact is a significant challenge. The Bison-CASL results presented in this report are based on glued contact between the pellet and clad for both the 2-D and 3-D simulations. This simplification will lead to higher than expected hoop stresses due to neglecting any slippage between the fuel

pellet and cladding. Also for the 3-D MPS model, it is assumed that the five pellets are merged together to prevent any asymmetric shifting of the pellet, which adds further complexities to the problem.

Figure 6 shows the power histories used within the calculations used to evaluate the cladding hoop stress. The power histories are idealized cases similar to PWR ramp tests. Both power histories contain an initial ramp up to 25 kW/m over the course of 2.8 hours, with a 24-hour hold period. This is followed by a final, linear ramp up to full power over one hour, again followed by a 24-hour hold period. The final linear power for the low burnup rod is 40 kW/m and for the higher burnup rod is 32.8 kW/m.

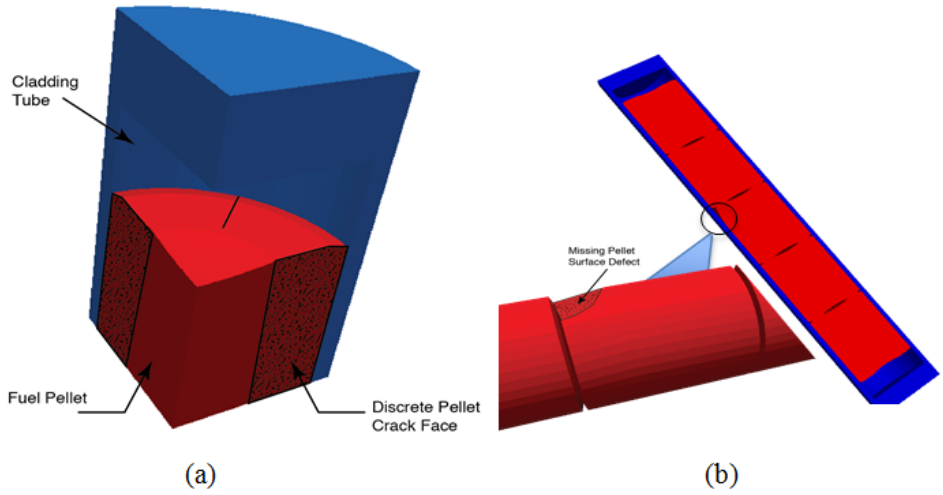


**Figure 5.** (a) 3-D geometric representation of a cracked pellet., and (b) 3-D geometric representation of a 5-pellet rodlet with the center pellet having an MPS defect.

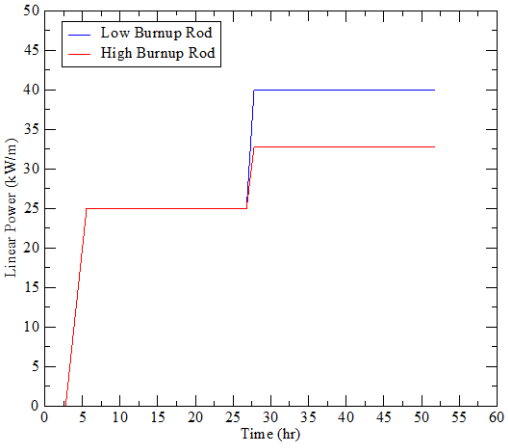


**Figure 6.** Power histories used to simulate the impact of discrete cracks and MPS on the local cladding hoop stress.

## 3. RESULTS OF PCI MODELING USING BISON-CASL

The assessment of the PCI capabilities consisted of four major areas of investigation; 2-D modeling of fuel pellet cracks, 2-D modeling of MPS defects, 3-D modeling of fuel pellet cracks, and finally, 3-D modeling of MPS defects. The primary purpose of these activities is to establish the relationship between the different methods used to model the pellet and cladding geometry and the resulting localized cladding stress distribution and magnitude.

The important factors that were evaluated included the length and frequency of discrete pellet cracks, the dimensions (width, depth, and length) of the MPS defect, the friction coefficient between the pellet and cladding, and the role of the out-of-plane mechanical loading for the 2-D R-theta models. Each of these parameters is varied separately (and some cases together) to determine the impact on the maximum cladding stress, the stress distribution, and the local temperature perturbations. Appropriately representing these conditions as a function of irradiation effects and power history are fundamental to any methodology that will be used for PCI assessments. The use of more mechanistic material damage models will require, as a starting point, the local stress and temperature distributions in order to calculate material flow, chemical reactions, and fracture behavior.

### 3.1 2-D R-Theta Modeling of PCI Effects

The purpose of the 2-D geometric modeling is to evaluate the local cladding stress concentration under various idealized geometry conditions as a means to parameterize the influence of different modeling approaches. In contrast to 2-D axisymmetric R-Z models used to represent a full-length fuel rod, the 2-D planar models represent a small slice of a fuel rod. Symmetry in the R-Theta plane is imposed by using reflective boundary conditions. The out-of-plane conditions result in approximations to address the mechanical constraints in the axial direction and also lead to infinitely long geometric configurations. These approximations will influence the calculated deformations and temperatures and part of the assessment below will highlight these effects and indicate potential approaches to minimize their impact on PCI assessments.

### 3.1.1 Fuel Crack Effects on Cladding Hoop Stress

Sensitivity studies have been performed to characterize the relationship between the size and angular spacing of discrete radial pellet cracks with the finite element mesh on the localized cladding stress distribution, using the 2-D R-Theta model shown in Fig 4a. First, the angular spacing of the pellet cracks was investigated. The 90° model was configured to have cracks at 0° and 90° (2 cracks); 0°, 45°, and 90° (3 cracks); and 0°, 30°, 60°, and 90° (4 cracks). In all three cases, the cracks extended to 50% of the pellet radius. Second, a R-theta model containing three cracks (0°, 45° and 90°) was modified to evaluate crack lengths ranging from 20% to 70% of the pellet radius.

The simulations were performed using the low burnup power history shown in Figure 6 with a cladding fast neutron fluence of $5x10^{25}$ n/m$^2$ and a residual pellet-cladding gap of 25 microns. The maximum cladding hoop stress calculated as a function of the angular spacing between the cracks by Bison-CASL is shown in Figure 7. In addition to the Bison-CASL results, select Falcon results are shown for two of the crack configurations. While the magnitude of the stress differs rather significantly, it can be argued that there is a trend towards saturating maximum cladding hoop stress with decreasing number of cracks in the clad (increased crack spacing).. It should also be noted that the Falcon calculations were performed using a coarser finite element mesh, which will have an important impact on the magnitude of the localized stress.

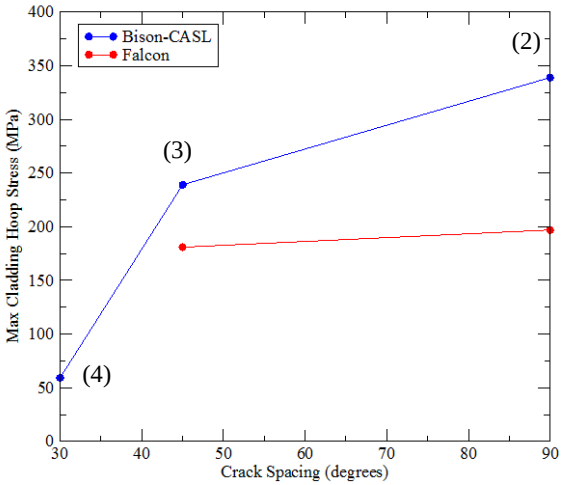


**Figure 7.** The maximum clad hoop stress calculated in a 2-D (R-Theta), 90 degree model as a function of the number of radial cracks.

In Figure 7, values obtained by the Bison-CASL code are shown in blue, as compared to values calculated by Falcon in red. The number of explicit cracks in the model is shown in parenthesis.

The results demonstrate that as the angular spacing between the cracks decreases, the maximum cladding hoop stress decreases as well. This trend is consistent with changes in the driving force responsible for the stress localization, i.e. the pellet crack opening displacements caused by thermal expansion. The high number of radial cracks present in the pellet reduces the crack opening displacement experienced by a single crack for a given amount of pellet thermal expansion, thus causing smaller shear forces at the pellet-cladding

interface [25]. Due to the simulated geometry, the cases analyzed with Bison-CASL represent 4, 8, and 12 radial cracks per pellet. Typical cracking patterns observed in post-irradiation examinations of commercial LWR fuel find between 6 and 10 radial cracks per pellet, as shown in Figure 1 and discussed by Oguma et al. [27]. Based on such PIE observations, the remainder of the Bison-CASL evaluations presented in this article will focus on the 3-crack 90° model. Furthermore, this geometry with 3 cracks had the best quantitative agreement in the maximum clad stress between the Falcon and Bison-CASL models.

Figure 8 displays the results of varying the radial crack length on the maximum cladding hoop stress distribution, as calculated in the 2-D (R-Theta), 90° model containing 3 cracks. The crack length was adjusted from 20% of the pellet radius to 70%. The results show that the maximum clad stress increases with increasing crack length, but trends towards saturation for crack lengths greater than 50% of the pellet radius. The 50% crack length corresponds to the case shown in Figure 7, for which Falcon calculated a maximum clad hoop stress of 175 MPa, slightly below the corresponding value of about 240 MPa using Bison-CASL. Increasing the crack length causes a decrease in the compliance of the fuel pellet, which allows the crack to open more during a power increase. With a larger crack opening displacement, there is a corresponding increase in the shear force transferred to the clad inner surface, thereby producing a larger clad hoop stress with increasing fuel crack length.

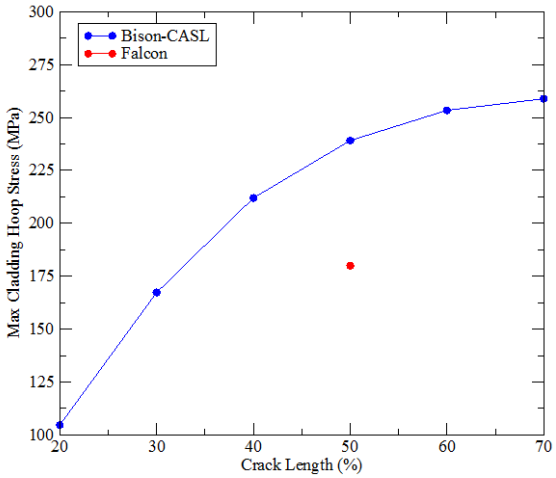


**Figure 8,** 2-D Bison-CASL R-Theta calculations of a 90-degree pellet containing 3 radial cracks showing the influence of crack length on the maximum clad hoop stress.

**Comment [BW1]:** I would remove the Falcon case --- only one data point and it was shown in Figure 10

The hoop stress contours within the cladding at the time of the maximum cladding stress (~30 hrs into the power history diagram shown in Section 2) for the 30%, 50%, and 70% crack length are shown in Figure 12 (a-b). These contours clearly indicate that the maximum hoop stress occurs at the position where the pellet crack impinges on the cladding. The magnitude of the stress intensity associated with the crack (e.g., maximum/minimum clad hoop stress) on the cladding inner surface displays a dependence on the crack length, varying from 2.2 in the case of the 30% crack to 2.7 in the case of the 70% crack.

The cladding hoop stress distributions and stress intensity are consistent with those calculated by Falcon and ALYCONE, which exhibit values ranging from 1.5 to 2.5 [5, 23-25]. Figure 10 shows the cladding stress concentration factor at the inner clad surface as a function of angular distance from the pellet crack location for the 70% crack length, as calculated by Bison-CASL and compared to Falcon calculation results reported by Lyon, et.al. [23]. The stress values have been normalized to the far-field stress to allow for a direct comparison between the results from Bison-CASL and the Falcon. Excellent agreement is seen between the distributions. Again, it is possible that the more refined finite element mesh density used in these Bison-CASL calculations contributes to the higher values seen at the crack tip location.

High tensile hoop stresses are observed at the pellet crack tip for both the 30% and 50% cases. These results indicate that the cracks would most likely extend deeper into the pellet for the pellet stress conditions calculated, if the model were able to extend the crack length mesh. Correspondingly, a key observation from this assessment is that a 70% long radial crack appears appropriate for use in modeling discrete crack behavior using the 2-D modeling approach.

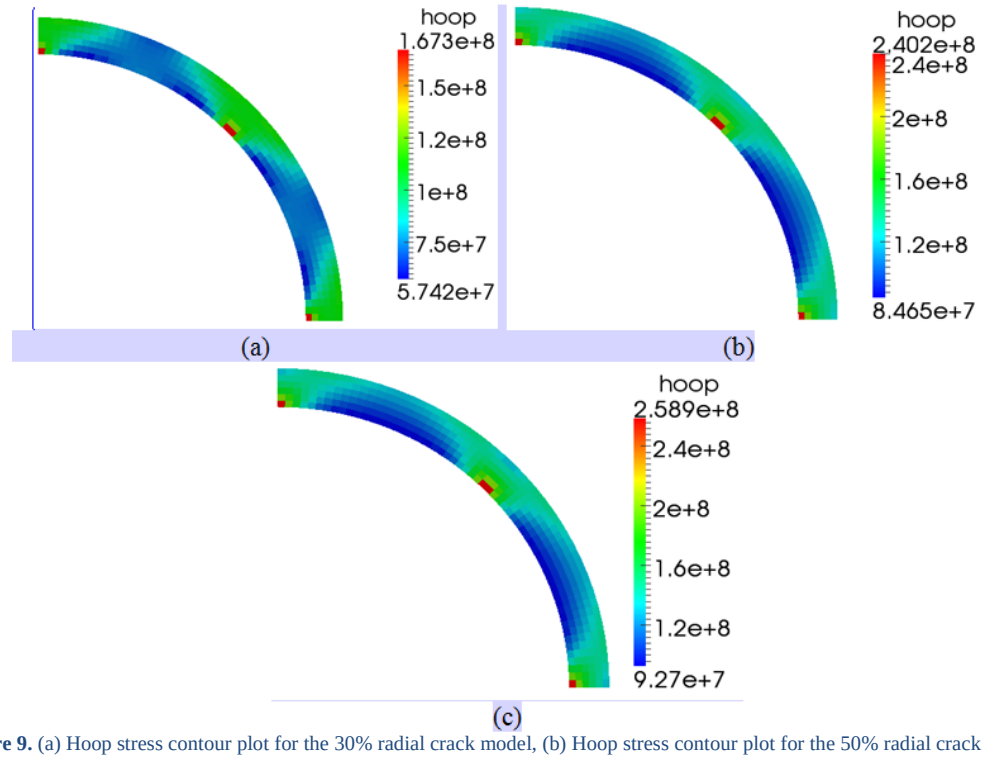


**Figure 9.** (a) Hoop stress contour plot for the 30% radial crack model, (b) Hoop stress contour plot for the 50% radial crack model, and (c) Hoop stress contour plot for the 70% radial crack model.

**Comment [BW2]:** Combine these into a single figure with parts a, b and c --- Please replot these with color scale denoted in MPa

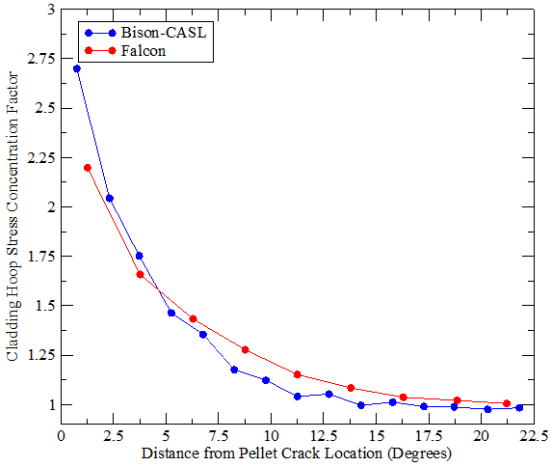


**Figure 10.** Clad hoop stress concentration factor as a function of the angular position from the fuel pellet crack location for a 70% long radial crack in a 2-D, R-Theta geometry.

**In Figure 10, the results from Bison-CASL are shown in blue, whereas values calculated by Falcon are shown in red. The stress concentration factor is defined as the ratio of the local stress to the minimum value of the stress far away from the crack. The Falcon results have been reproduced from Ref. [23].**

### 3.1.2 MPS Defect Effects on Cladding Hoop Stress

The mechanisms driving the increase in cladding failure potential is similar for an MPS, but the path to cause failure is significantly different. As discussed above, pellet cracks open during a power increase and induce a shear force on the cladding, which can lead to failure in the case of classical PCI. However, with an MPS defect, the local cladding region adjacent to the MPS defect does not come into contact with the fuel pellet. Thus the maximum hoop stress results bending stresses in the regions surrounding the MPS defect. Further, local temperature perturbations due to low heat transfer across the larger gap volume impact both the maximum cladding hoop stress (higher fuel temperatures leading to greater thermal expansion) and the stress relaxation behavior (lower cladding temperatures).

Figure 4 (a) shows a schematic of the 2-D planar R-Theta model used in Bison-CASL to calculate the complex thermal and mechanical conditions associated with the presence of an MPS defect. A 2-D, planar R-Theta model with 180° symmetry is used to represent the geometry of a pellet containing an MPS defect. Symmetry is imposed at the 0º and 180º positions and 3 pellet cracks are included at 0º, 90º and 180º positions and are represented by mechanically free surfaces extending 70% of the pellet radius.

Two different MPS defect geometries were included in this assessment: a flat-faced defect and a concave defect. PIE observations of MPS defects have found both types present in LWR fuel. The width of the MPS defect was varied from a small size of 45 mils (1.1 mm) to a large size of 150 mils (3.8 mm). These values span the range from below an acceptable MPS defect to the size observed to cause cladding failure.

Because of the 2-D representation, the length of the MPS defect is infinitely long (in the out-of-plane direction), which produces an exaggerated effect on the temperature and stress condition. The impact of a finite length MPS defect requires a 3-D model as will be discussed later.

The MPS defect width or angle subtended by the missing circumferential surface affects the length of the unsupported cladding tube once contact occurs elsewhere along the interface. Both the width and the curvature also influence the distance between the pellet surface within the MPS defect and the cladding inner surface. This distance or gap has an important impact on the heat transfer from the pellet to the cladding, and results in a hotter region in the pellet adjacent to the MPS defect and a cooler cladding region. Examples of representative non-uniform temperature distributions are shown in Figure Y for the 45-mil and 150-mil flat MPS defect cases, respectively. In both of these simulations, the temperature distributions are shown at the time of the peak cladding stress, which occurred at a power level of 40 kW/m in Figure 11 (a) and 40 kW/m in Figure 11 (b)

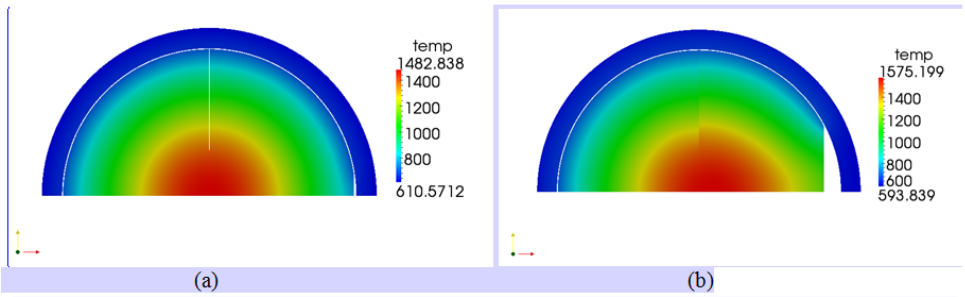


**Figure 11.** (a) Temperature Contour at Peak Cladding Stress Time for a 45-mil Flat MPS Defect, and (b) Temperature Contour at Peak Cladding Stress Time for a 150-mil Flat MPS Defect.

**Figure 11.**

**Comment [BW3]:** Combine into single Figure with parts a) and b)

The maximum cladding hoop stress and maximum fuel centerline temperature are shown in Figure 12 as a function of MPS width (represented by the subtended angle). The maximum cladding hoop stress increases as the width of the MPS defect increases. These results are consistent with the increase in the bending moment experienced in the cladding as the unsupported cladding length increases for larger MPS defects. An apparent saturation in this stress level is observed as the MPS size increases towards 50°. Several factors maybe responsible for the saturation of the cladding hoop stress with large MPS defects, including thermal creep within the fuel pellet and geometric effects associated with the unsupported cladding region.

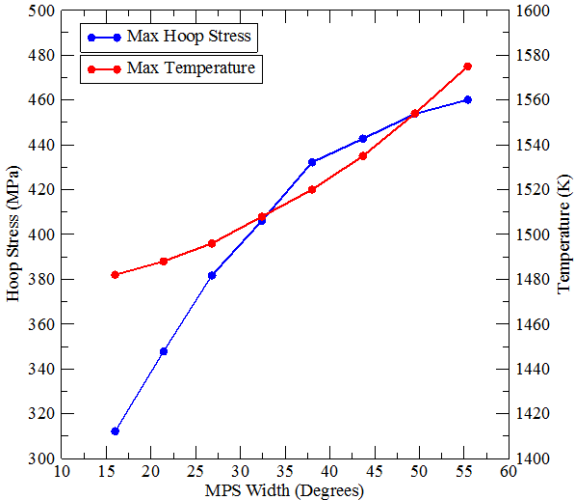


**Figure 12.** 2-D Bison-CASL calculations of a 180 degree pellet containing 3 radial cracks of 70% length, and a MPS, which shows the affect of increasing the MPS width on the maximum clad hoop stress (blue curve) and maximum fuel centerline temperature (red curve).

EPRI has previously used the Falcon fuel performance code to calculate the stress concentration in the cladding due to MPS defects [3]. In that work, the stress concentration factor was defined to be the ratio of the maximum cladding hoop stress for a given MPS defect divided by the maximum cladding hoop stress calculated for the same conditions of geometry, gap thickness and power history without an MPS defect. Both calculations used 2-D planar R-Theta models similar to those discussed in Section 2. The Falcon results were provided to CASL for comparison to the results from Bison-CASL [3].

Following that approach, we have also calculated the 2-D MPS stress concentration factors using Bison-CASL for a flat MPS defect geometry, containing 3, 70% long pellet cracks in a 2D, R-Theta 180° geometry. Figure 13 shows a comparison of the Bison-CASL and Falcon 2-D stress concentration factors as a function of MPS defect size. The trend is consistent between the two codes, that is, as the MPS defect size increases, the stress concentration factor also increases. The most notable difference is the fact that for large MPS defects, the Bison-CASL results display a much stronger saturation behavior. Possible causes of this behavior could be the treatment of the out-of-plane (axial) mechanical boundary conditions, differences in the $UO_2$ thermal creep behavior, as well as differences between the geometric representation of the MPS used, Bison-CASL assumed a flat MPS whereas Falcon assumed a concaved. However, overall, the results of the comparison of the calculated MPS stress concentration factor in 2D are quite consistent between the Bison-CASL and Falcon calculations.

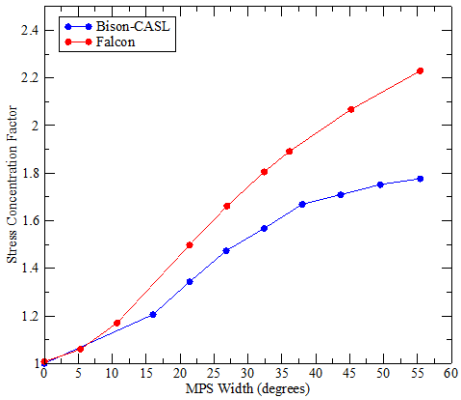


**Figure 13.** 2-D Stress concentration factor, as a function of MPS defect width compared to values from the literature [3].

However, there are quantitative differences between the calculated stress concentration factor using Falcon and Bison-CASL, as shown in Fig. ZZ. A significant difference is the shape of the MPS simulated in the two models. Falcon assumed a concave-shaped MPS, while the Bison-CASL model used a flat MPS. Figure 14 summarizes the results of Bison-CASL calculations that compare the impact of flat and concave MPS defects, as a function of MPS width. From Figure 14, it can be seen that as the MPS defect width increases, the maximum cladding hoop stress increases, and that the maximum pellet temperature increases. Both the bending moment due to the unsupported cladding tube and the large thermal expansion of the pellet are responsible for the increase in maximum hoop stress with increasing MPS size. The fuel temperature is also increased by the concave MPS defect geometry. These results clearly indicate that a curved MPS with concave geometry will produce both higher fuel centerline temperatures and larger maximum hoop stresses, for a fixed MPS size. This is consistent with the lower calculated stress concentration factor using Bison-CASL as compared to Falcon in Figure 13.

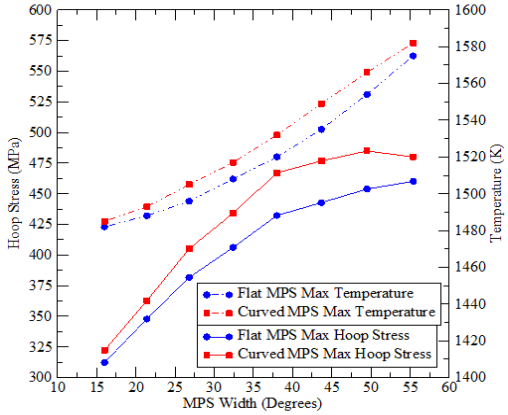


**Figure 14.** Cladding Stresses Calculated by Bison-CASL for Various Size MPS Defects, along with the Corresponding Maximum Temperature in the Fuel Pellet.

The more realistic, concave geometry of the MPS used in Figure 14 should improve the comparison of the Bison-CASL calculated results to those of Falcon, but that was not the only difference in the results shown in Figure 13. to Falcon, however Falcon also used a 90 degree model containing crack lengths of 50% of the fuel radius. Figure 24 summarizes a Bison-CASL comparison assuming a 90 degree model containing a concave MPS with two radial cracks of length 50% of the fuel radius. The comparison between Bison-CASL and Falcon are astounding, however the assumptions used in the Falcon results are inherently flawed. By assuming a 90 degree model, symmetry tells us that the pellet contains two MPS. The assumption of two MPS causes an increase in the maximum fuel temperature, which in turn increases the thermal expansion of the pellet. The increase in thermal expansion gives rise to higher induced shear stresses in the cladding. Furthermore, Falcon assumes the lengths of the cracks to be 50% of the fuel radius. Bison-CASL analysis shows hoop stress at the crack tip to be higher than the critical stress of $UO_2$. With the calculated hoops stress being higher than the materials critical stress would lead to elongation of the radial cracks. For this reason longer cracks are needed to more accurately model the phenomenon of PCMI. However to get a accurate comparison to Falcon, Bison-CASL used a 90 degree model containing radial cracks 50% in length and a concaved MPS. The results of the one to one comparison can be seen in Figure 15. Bison-CASL and Falcon agree very well with each other but diverge when the MPS becomes significantly large. It is unclear what the cause of this divergence is.

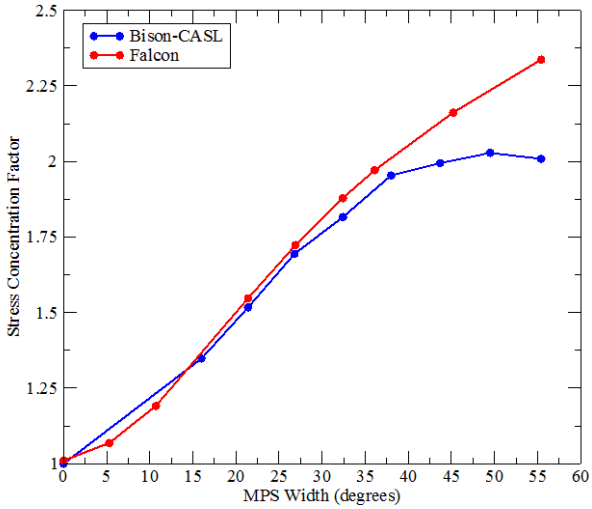


**Figure 15.** 2-D Stress concentration factor using the same geometric models, e.g. crack length, MPS shape, and 90 degree model, as a function of MPS defect width compared to values from the literature [3].

Another study was conducted to simulate a higher burnup rod. In this analysis, we have further reduced the pellet-clad gap, for both the MPS models as well as the 70% pellet crack model, and lowering the power seen in Figure 6. The purpose of this study is to analysis how the changes in the stress values would change the 2-D stress concentration factor. The same methodology was used to determine the 2-D MPS stress concentration factors. Figure 16 shows the comparison between the lower burnup rod and the higher burnup rod. By running the same analysis study it clear shows the stress concentration is unaffected by the change is stresses. This result points to a scaling relationship between the PCI stresses and the stresses induced by MPSs.

**Comment [BW4]:** This needs to be explained more clearly --- Is the second Fig 24 using 180° symmetry – what exactly are the gap and fluence values for the high burnup rod --- what burnup would that correspond to?

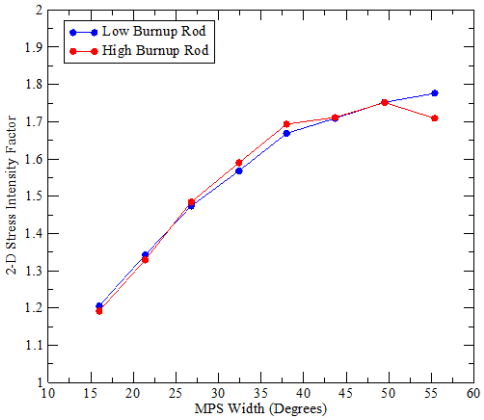


**Figure 16.** Comparison of 2-D Stress concentration factor for a low burnup rod and a high burnup rod, as a function of MPS defect width.

### 3.2 3-D Five Pellet Model with MPS Defect

Modeling the geometric conditions of a MPS defect in 3-D requires multiple pellets to appropriately represent the mechanical boundary conditions. A finite element mesh with a stack of five (5) pellets within a cladding tube, where the central pellet contained an MPS defect extending partway down the length of the pellet was generated, and presented earlier in in Figure 5. The model consisted of a 180° representation, with the symmetry plane passing through the mid-line of the MPS defect. The symmetry planes were also configured to include a pellet crack that is 50% of the pellet radius (at 0° and 180° positions). Difficulties in the contact algorithm used in MOOSE prevented the inclusion of pellet cracks at other locations (45°, 90°, or 135°) in the finite element mesh. The model shown in Figure 7 contains a 105-mil wide by 105-mil long flat MPS defect. Table 1 lists the MPS defect sizes used in the assessment. A total of five MPS defects with flat surfaces of equal width and length dimensions (W/L = 1) were analyzed with Bison-CASL.

Figure 17 contains a comparison of the inner surface cladding hoop stress as a function of time for the 2-D and 3-D models containing an MPS defect with a width of 105 mils. The 2-D results, shown in blue, exhibit a higher clad stress as compared to the 3-D results. The largest contribution to the difference between the 2-D and 3-D calculations is the fact that the 2-D model represents the MPS defect to be infinitely long with a finite width, whereas the 3-D model explicitly includes the MPS defect with a finite length and width. The finite length of the MPS reduces the bending forces by providing additional support in the axial direction that is not included in the 2-D model.

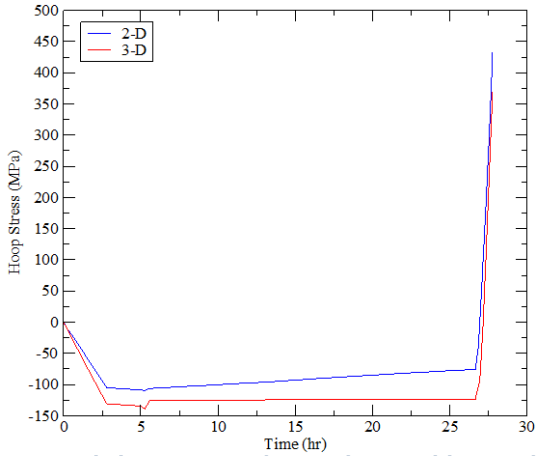


**Figure 17.** Comparison of the hoop stress calculations a 2-D R-Theta 180 degree model MPS with a width of 105 mil (blue line) to a 3-D 180-degree model containing a MPS of width 105 mils and length of 105 mils (red line).

**Comment [BW5]:** Again, need to describe where you are comparing the 2- to 3-D hoop stress values

Figure 18 (a-c) displays the temperature distribution in the fuel pellet, the temperature distribution in the cladding and the inner cladding surface hoop stress contour, respectively for the 5-pellet 3-D model containing a 105 x 105 square-mil MPS defect at a time corresponding to the maximum hoop stress. These results illustrate the complex effects caused by the MPS defect, such as ….. The pellet-pellet interface and the MPS defect location are easily discernable from the contour plots.

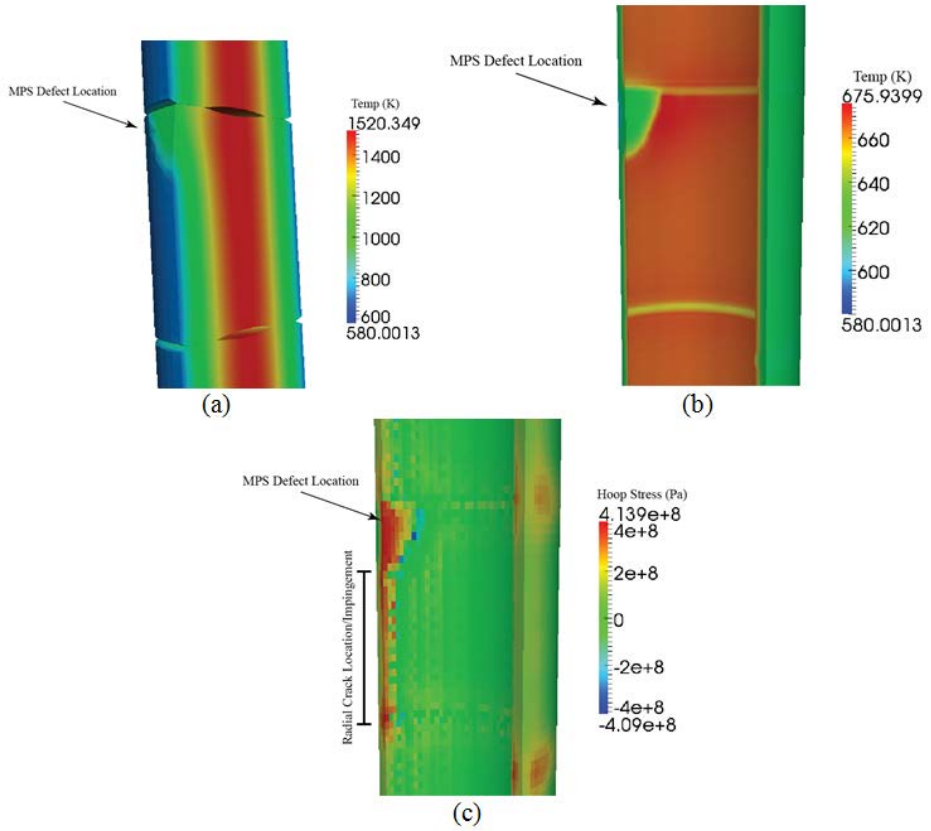


**Figure 18.** (a) Pellet temperature distribution in the vicinity of the MPS defect, (b) Inner cladding surface temperature distribution in the vicinity of the MPS defect, and (c) Inner cladding surface hoop stress distribution in the vicinity of the MPS defect.

Previous experience with structural analysis assessments have shown that the hoop stress should increase as a function of the MPS volume increases. Table 1 lists the maximum cladding hoop stress calculated for different MPS defect sizes, all modeled with a width to length ratio (W/L) equal to unity. The maximum cladding hoop stress from Bison-CASL is calculated to increase with larger MPS defects, similar to that observed from the 2-D MPS defect stress results. Furthermore, the cladding stresses calculated with the 3-D model are 7-16% lower than those from the 2-D model due to the axial length effect. This is shown by the ratio of 3-D to 2-D maximum stress values in Table 1. The comparison of the 3-D and 2-D stress calculations highlights the inherent 3-D effects of an MPS defect on the cladding stress state. The results obtained by EPRI using the ABAQUS general-purpose structural analysis code are shown in Table 1. Excellent agreement is found for the geometric effect on the maximum cladding hoop stress for a finite length MPS defect between Bison-CASL and ABAQUS.

**Table 1.** 3-D Bison-CASL maximum hoop stress calculations as a function of MPS defect width, with a W/L = 1, and ratio of the maximum 3-D hoop stress to the maximum 2-D hoop stress.

| MPS Defect Width (mils) | Max Hoop Stress (MPa) | Bison-CASL $\sigma_{3\text{-}D}/\sigma_{2\text{-}D}$ | EPRI/ABAQUS $\sigma_{3\text{-}D}/\sigma_{2\text{-}D}$ |
|---|---|---|---|
| 45 | 311 | 1.0 | .94 |
| 60 | 348 | 1.0 | .92 |
| 75 | 357 | 0.93 | 0.89 |
| 90 | 362 | 0.89 | 0.88 |
| 105 | 369 | 0.85 | 0.86 |
| 120 | 375 | 0.84 | 0.84 |
| 135 | 387 | 0.85 | N/A |
| 150 | 406 | .88 | N/A |

Calculating stresses induced by a finite dimension MPS defects is an important step in developing a methodology to model cladding failure using fuel behavior modeling. One approach is to use 2-D fuel performance codes like Falcon or RODEX-4 and then apply stress intensification factors determine from a structural mechanics analysis. This approach as been used by EPRI and AREVA to estimate the maximum cladding stress using classical PCI stress analysis methods and then applying MPS defect stress concentration factors as a function of MPS defect size [3, 13]. Figure 19 compares the 3-D stress concentration factors from the Falcon/ABAQUS calculations performed by EPRI and ANSYS calculations performed by AREVA with those obtained from the Bison-CASL assessment using the 3-D 5-pellet model. This comparison demonstrates good consistency in capturing the MPS defect size effect on the stress concentration factor. Noticeable differences are seen between the absolute values of the stress concentration factors. These differences are most likely related to the approaches used in the stress analysis of fuel pellet cracks, which form the basis for the classical PCI methods used in Falcon and RODEX-4.

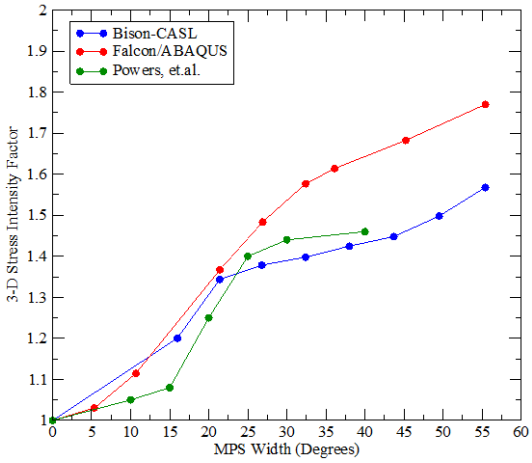


**Figure 19.** 3-D Bison-CASL stress concentration factor, as a function of MPS defect width, compared to values from literature [3,13].

# 4. SUMMARY AND CONCLUSIONS

The results of this assessment have demonstrated that the pellet cladding mechanical interaction (PCMI) 2-D and 3-D modeling capabilities in Bison-CASL are consistent with PCI modeling approaches used by EPRI in the Falcon fuel behavior code [2, 3] and CEA with the ALCYONE code [4]. By representing idealized cracked or defected pellet geometries using 2-D and 3-D finite element meshes, Bison-CASL is able to calculate the local stress distributions at the clad inner surface that are important for determining the initiation and propagation of stress corrosion cracks. This preliminary work on modeling fuel cracks and MPS in a full 3-D representation finds that 3-D geometric effects must be considered for mechanistic evaluations of PCI failure with MPS defects.

The Bison-CASL and Falcon 2-D stress concentration factors as a function of MPS defect size were compared and the trend is consistent between the two codes, that is, as the MPS defect size increases, the stress concentration factor also increases. The most notable difference is that for large MPS defects, the Bison-CASL results display a much stronger saturation behavior. Possible causes of this behavior could be the treatment of out-of-plane (axial for 2-D R-Theta) mechanical boundary conditions and differences in the $UO_2$ thermal creep modeling. However, the consistency in the behavior of the 2-D results between Bison-CASL and Falcon demonstrates that the CASL development efforts are progressing in the right direction.

The comparison of the 3-D cladding stress calculations with those obtained by others show excellent agreement for the geometric effect on the maximum cladding hoop stress for a finite length MPS defect. Stress reduction factors of 7 to 16% for finite length MPS defect were calculated by Bison-CASL using a 5-pellet model, which agreed closely with those calculated by EPRI using ABAQUS. When applying these factors to the 2-D stress calculations, the Bison-CASL results correlate closely with those published by AREVA and are lower than those reported by EPRI.

Further work on Bison-CASL will focus on integrating micro-scale models under development in CASL-MPO that describe the irradiation creep and growth of zirconium alloys, the fracture, relocation, and mechanical compliance of the fuel pellet, and the release of fission products important for SCC (volatile and noble gases). The incorporation of these models into Bison-CASL, either directly or using improved semi-empirical relationships, will require expanding the validation activities of Peregrine to include integral fuel rod irradiations at Halden, hot-cell examination data from commercial reactor fuel rods, and separate effects experiments.

## REFERENCES


1. R. O. Montgomery et al, “Peregrine: Validation and Benchmark Evaluation of Integrated Fuel Performance Modeling Using Test Reactor Data and Falcon,” L1.CASL.P7.02., June, 2013
2. Fuel Analysis and Licensing Code: Falcon MOD01: Volume 1: Theoretical and Numerical Bases, EPRI, Palo Alto, CA: 2004. 1011307.
3. Fuel Reliability Guidelines: Pellet-Cladding Interaction. EPRI, Palo Alto, CA: 2008. 1015453
4. Sercombe,J., Michel,B., Thouvenin,G., Petitprez,B., Chatelet,R., Leboulch,D., Nonon,C., 2009. Multi-dimensional modeling of PCMI during base irradiation and ramp testing with ALCYONE V1.
5. J. Rashid et al, “Modelling of PCI under steady state and transient operating conditions,” Technical committee on water reactor fuel element computer modelling in steady state, transient and accident conditions, Preston (UK) 18-22 Sep 1988, pp. 91-101
6. Brian Cox, “Zirconium Alloy Fuel Cladding – A Review,” Journal of Nuclear Materials, 172 (1990) 249-292
7. M. F. Lyons, D. H. Coplin and C. G. Jones, GE Quarterly Progress Reports, GEAP - 3771-10 to -12 (1963/64)
8. J.T.A. Roberts and F.E. Gelhaus, “Zircaloy Performance in Light Water Reactors,” Zirconium in the Nuclear Industry (Fourth Conference), ASTM STP 681, ASTM, 1979, pp. 19-39
9. F. Garzarolli, R. von Jan, H. Stehle, The Main Causes of Fuel Element Failure in Water-Cooled Power Reactors, Atomic Energy Review, **17**, 1 (1979)
10. Gittus, J.H., “Theoretical analysis of the strains produced in nuclear fuel cladding tubes by the expansion of cracked cylindrical fuel pellets,” *Nucl. Eng. Des.* 18, 69–82, 1972.
11. F. Groeschel, G. Bart, R. Montgomery, S. K. Yagnik, “Failure Root Cause of a PCI Suspect Liner Fuel Rod”, IAEA Technical Meeting on Fuel Failure, Bratislava, Slovakia, 17-21 June 2002
12. Y. Alyeshin et al, “The Effect of Pellet and Local Power Variations on PCI Margin,” Proceedings of the Topfuel 2010 LWR Fuel Performance Meeting, Orlando, US, September 26-29, 2010.
13. Chris Powers, Peter Dewes, and Michel Billaux. "Hot cell examination results of non-classical PCI failures at La Salle," Proceedings of the Water Reactor Fuel Performance Meeting 2005, Kyoto, (2005).
14. B.W. Spencer et al, "3D Simulation of Missing Pellet Surface Defects in Light Water Reactor Fuel Rods," Proceedings of the TopFuel 2012 Reactor Fuel Performance Conference, Manchester, United Kingdom, September 2-6, 2012
15. Sylvie Lansiart and Bruno Michel, Pellet Cladding Interaction, Nuclear Fuels, CEA Nuclear Energy Division Monograph, Jean-François Parisot, Ed, CEA, 2009.
16. Montgomery, R., et al., "Peregrine: Advanced Modeling of Pellet-Cladding Interaction (PCI) Failure in LWRs," Proceedings of the TopFuel 2012 Reactor Fuel Performance Conference, Manchester, United Kingdom, September 2-6, 2012
17. Ranjan, G.V., Smith, E., Determination of stress within zircaloy cladding due to pellet cladding interaction. Nucl. Eng. Des. 56, 263–272, 1980.
18. Roberts, G., The concentration of stress in cladding produced by the expansion of cracked fuel pellets. Nucl. Eng. Des. 47, 257–266, 1978.
19. *ABAQUS/Standard User’s Manual, Vol. I & II* (ver. 5.4),(1994). Hibbit, Karlsson & Sorensen, Inc., Pawtucket, Rhode Island.
20. ANSYS R&D Inc., “ANSYS Manuals,” 2010.
21. D. Gaston, C. Newman, G. Hansen, and D. Lebrun-Grandie, “MOOSE: parallel computational framework for coupled systems of nonlinear equations. Nucl. Eng. Design,” 239, p. 1768–1778, 209.

22. R. Williamson, J. Hales, S. Novascone, M. Tonks, D. Gaston, C. Permann, D. Andrs, and R. Martineau, “Multidimensional multiphysics simulation of nuclear fuel behavior,” *Journal of Nuclear Materials* 423 (2012) 149–163.
23. W. Lyon, R. Montgomery, Y. Rashid, “PCI Analysis and Fuel Rod Failure Prediction using FALCON,” Proc. TOPFUEL ’09, Paris, France, 2009.
24. B. Michel, J. Sercombe, G. Thouvenin, "A new phenomenological criterion for pellet cladding interaction rupture," *Nuclear Engineering and Design* 238 (2008) 1612–1628.
25. N. Marchal et al, “Finite element simulation of Pellet-Cladding Interaction (PCI) in nuclear fuel rods,” *Computational Materials Science*, 45 (2009) 821-826.
26. S. P. Timoshenko and J. N. Goodier, Theory of Elasticity, McGraw-Hill, 1970
27. Masaomi Oguma, “Cracking and Relocation Behavior of Nuclear Fuel Pellets during Rise to Power,” *Nuclear Engineering and Design* 76 (1983) 35-45.
28. J. C. Wood, B. A. Surette, I. Aitchison and W. R. Clendening, “Pellet Cladding Interaction – Evaluation of Lubrication by Graphite,” *Journal of Nuclear Materials*, 88 (1980) 81-94.